CHEMISTRY OF MATERIALS

ARTICLE

pubs.acs.org/cm

Investigation of the Photocross-Linking Mechanism in Oxetane-Functionalized Semiconductors

Stephan Feser[†] and Klaus Meerholz*[,†]

[†]Chemistry Department, University of Cologne, Luxemburger Str. 116, 50939 Cologne, Germany

Supporting Information

ABSTRACT: Oxetane-functionalized organic semiconductors have been used for fabricating multilayer OLEDs from solution and for lithographic patterning. These materials are commonly cross-linked photochemically by cationic ring-opening polymerization (CROP) in the presence of a photoacid generator (**PAG**). Due to the sensitization of the reaction by the semiconductor itself, illumination leads to the photoinduced electron transfer (PET) from the **PAG** to the semiconductor. This in turn leads to — besides the intended cross-linking — redoxchemical doping of the layers, which may have an important impact on the device performance. Until now, the exact quantities of this unintentional side reaction were unknown. In this study, we use organic field-effect transistors to investigate and quantify the mechanism of photosensitized cross-linking of oxetane-functionalized organic semiconductors. By comparing the compound of interest, for example, a derivative of the commonly used hole conductor triphenylamine dimer (TPD), with an almost identical, noncross-linkable TPD-derivative and by using a quantitative oxidant in comparison with the **PAG**, we were able to quantitatively assign all possible reaction pathways. Furthermore, the experiments provide detailed information of the charge transport characteristics of doped cross-linked films. The charge-carrier mobility increases with the doping level by a factor of up to two. It turns out that the **PAG** induces a stoichiometric fraction of mobile charge-carriers of 2.5×10^{-4}. Finally, it is shown that thermal annealing of cross-linked films leads to controlled dedoping of the semiconductor.

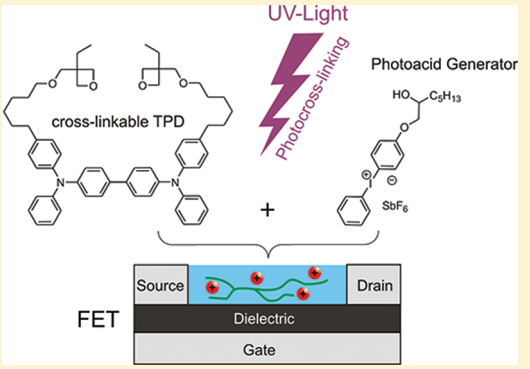

KEYWORDS: oxetane, ring-opening polymerization, organic semiconductors, doping

1. INTRODUCTION

Organic light-emitting diodes (OLEDs) are among the competing technologies for future display and solid-state lighting applications. To date, best performing OLEDs are based on small-molecule materials, where commonly several layers are vapor deposited in ultra high-vacuum.[1] On the one hand, this proceedure benefits straightforward processing and highly purified layers, but on the other hand it is very time- and energy-consuming. For cost-effective production, it is preferable to process from solution, e.g. by printing. However, usually multilayer structures are required to ensure acceptable device performances. To prevent interface mixing and erosion by consecutive layer deposition from solution two fundamental approaches have been followed.[2] The first one is to use orthogonal solvents for each individual layer.[3] This is however limited, since only few solvents can be used to dissolve typical materials.[4,5] In the second approach cross-linkable materials are employed, which become insoluble in a subsequent treatment step.[6,7]

Among the various options for cross-linkable materials, oxetane-functionalized organic semiconductors have been used for fabricating multilayer OLEDs from solution and for lithographic patterning. These materials are commonly cross-linked photochemically by cationic ring-opening polymerization (CROP) in the presence of a photoacid generator (**PAG**) such diaryliodonium salts generating an electrophilic species under UV-irradiation (Figure S1, Supporting Information).[8] However, the interplay between **PAG** and the oxetane-functionalized semiconductor is rather complex and leads to several reaction pathways, which can notably affect the device performance. Scheme 1 shows the proposed reaction scheme of a frequently used oxetane-functionalized hole-conductor **HMX** (also referred to as OTPD[9]) in conjunction with the **PAG**. The cross-linking process can be roughly divided into two steps:

(1) Initiation: The activation of the **PAG** in a hole-conductor matrix implicates a sensitized photolysis, Scheme 1b. By illuminating with UV-light the conjugated aromatic system of **HMX** acts as sensitizer owing to absorption at longer wavelengths than the **PAG** absorption (for spectra see Figure S2). The strong spectral overlap between light source and **HMX** facilitates an efficient photoexcitation of the hole-conductor followed by a subsequent photoinduced electron transfer (PET) to the **PAG**. This PET is assumed to be quantitative regarding the **PAG**, since a large excess of the sensitizer (the compound to be cross-linked itself) is provided. Note, that in contrast to commonly

Received: August 8, 2011
Revised: October 5, 2011
Published: October 20, 2011

Scheme 1. (a) Chemical Structures, (b) Photoinduced Electron Transfer (PET), for Simplification the Counter Ion of the PAG Was Neglected, and (c) Proposed Follow-up Reaction Scheme

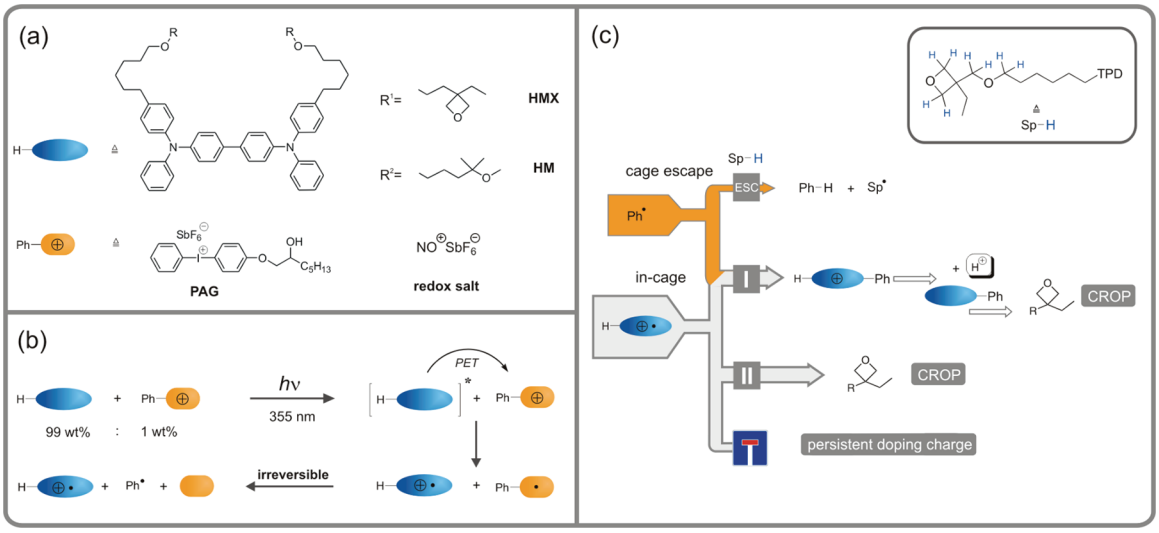

sensitized photolysis about 99 wt % sensitizer is present. The radical cation of the **HMX** hole conductor and a highly unstable **PAG** radical are formed, which in turn decomposes very fast and irreversibly to a phenyl radical and a neutral, iodinated species.[10] Here, the competing electron back transfer is neglected, since the light exposure for several seconds should in principle ensure a quantitative conversion.

(2) Follow-up reactions: the highly reactive phenyl radical and the **HMX** radical cation are then able to undergo several follow-up reactions, leading (a) to the desired CROP reaction or (b) to undesirable side reactions, Scheme 1c.[11,12] The phenyl radical and the **HMX** radical cation may combine with each other (presumably in-cage), and under rearomatization a proton is generated, which is then able to initiate the CROP reaction, pathway **I**. Alternatively, the **HMX** radical cation, being an electrophile itself, may directly initiate the CROP reaction, pathway **II**. This pathway is favored, if the phenyl radical undergoes typical cage-escape side reactions, such as CH-abstraction of H-atoms in α-position toward an ether unit of **HMX** moieties, pathway **ESC**. Finally, there is a certain probability that the formed **HMX** radical cations do not react further but instead remain in the **HMX** matrix as persistent (redox chemical) doping charge (symbolized by the dead-end sign, Scheme 1).

In this study, we demonstrate the quantitative detection of all reaction pathways. We utilize organic field-effect transistor (OFET) devices as testbed for a selective detection of the mobile persistent charge, corresponding to the dead-end pathway. Using a combinatorial experiment, the reaction pathways **I** and **II** can be addressed systematically. Therefore, in addition to **HMX** and the commonly used **PAG** {4-[(2-hydroxytetradecyl)-oxyl]phenyl}phenyliodonium hexafluoro-antimonate (**OPPI**), the noncross-linkable hole conductor **HM** and the one-electron oxidant nitrosylium hexafluoro-antimonate (**NO+**) are applied, Scheme 1a. In a second part, the charge (hole) transport properties of the cross-linked films is examined in detail and the impact of redoxchemical doping investigated.

2. EXPERIMENTAL SECTION

The FET devices used in this study are based on prefabricated Si^{2+}/SiO_2-substrates (Fraunhofer IPMS, Dresden). The substrates were patterned with 50 nm gold source/drain electrodes. The channel length L and width W were 2.5 μm and 1 cm, respectively. The silicon oxide used as dielectric had a layer thickness of 230 nm and an areal capacitance C_i of 15 nF/cm^2. The substrate was treated with hexamethyldisilazane (HMDS) prior deposition of the hole conductor to make the SiO_2-surface hydrophobic. The transistors were completed by spin coating 50 nm films of in-house synthesized hole conductor **HMX** and **HM**,[9] respectively, from toluene solution on silicon substrates.

Films added with **PAG** were fabricated under red light by mixing 12 g/L stock solutions of both, hole conductor and **OPPI** (Aldrich) from toluene solution immediately before spin coating. The resulting films were irradiated with 366 nm light for 10 s and cured at 100 °C for 2 min. Films added with stoichiometric dopant were prepared by mixing **NO+** (Aldrich) dissolved in nitromethane (12 g/L) with a toluene stock solution of hole conductor (12 g/L) immediately before spin coating and cured at 100 °C for 2 min. The NO radicals generated during the reaction are volatile. Soft curing at 100 °C was done to completely cross-link the layers (no longer soluble in any solvent).

The film thicknesses were measured with a Dektak 3 surface profilometer. Transistor characteristics were detected with an Agilent B1500A semiconductor analyzer. All transistor fabrication and measurements were carried out under inert nitrogen atmosphere.

3. RESULTS AND DISCUSSION

3.1. Quantifying Reaction Pathways. By implementing **HM** or **HMX** into an OFET we were able to detect its permanent charge-carrier density, which correlates with the amount of persistent doping charges and, accordingly, the dead-end pathway (Figure S3). With the known fraction of the dead-end and a systematic addressing of the other pathways, we were able to quantify the complete reaction pattern of **HMX** and **PAG** according to Scheme 1c.

Calibration. For the quantification of the number density of mobile charges in the films, a calibration was performed. Therefore, we used the noncross-linkable compound **HM** added with the one-electron oxidant **NO+** as reference system (see Figure S4). We

dx.doi.org/10.1021/cm202327c |*Chem. Mater.* 2011, 23, 5001–5005

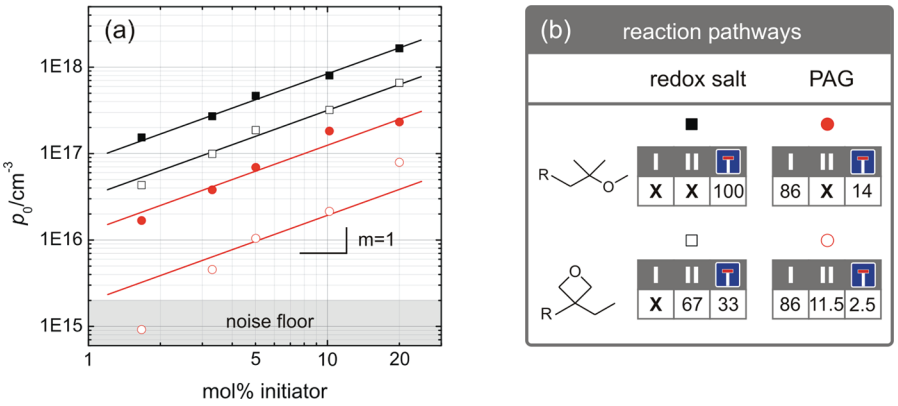

Figure 1. (a) Charge-carrier densities of **HMX** (open symbols) and **HM** (closed symbols) films added with different amounts of redox-salt (squares) and **PAG** (circles). The lines are fits with a slope of unity, indicating stoichiometric doping. The gray-shaded area illustrates the resolution limit of the current detection from the transistor measurements ("noise floor"). (b) Addressing rates of the reaction pathways derived from the offset of the lines in (a); see text for details. Pathways labeled with **X** are closed for the corresponding system. Noncross-linkable **HM** added with redox-salt serves as calibrating system, i.e. addressing only the permanent mobile charges, so-called "dead-ends".

found a linear dependence of the detected charge-carrier density p_0 on the initial loading of the initiator, the slope being unity (Figure 1a, solid black squares).

Photochemically Induced Reaction. We first consider reaction pathway **I**. Its existence was proven by first detecting the in-cage reaction product, the phenyl adduct of **HM**, by ESI mass spectrometry (Figure S5), and second by detecting the generated protons by adding an appropriate UV/vis indicator (Coumarin 6, Figure S6). To quantify pathway **I**, we used the noncross-linkable **HM** added with **PAG**. In this configuration pathway **II** is closed due to absence of reactive oxetane-functionalities. Consequently, either persistent doping charges (dead end) or protons are generated (pathway **I**). The detected charge-carrier densities revealed a doping level, which is lowered to 14% compared to the calibration, Figure 1a (solid red circles). Thus, it can be concluded that 86% followed pathway **I**.

The fraction of doping charge, which initiates the CROP following pathway **II**, is deduced from the mobile charge-carrier density of **HMX** films added with **PAG**. Owing to the identical electronic properties of **HM** and **HMX** the proton formation and photodoping rates are essentially identical. Hence, for **HMX** we assumed 86% for pathway **I**, as was determined for **HM**. The detected charge-carrier densities indicated a doping level of 2.5% for **PAG**-cross-linked **HMX**, Figure 1a (open red circles). Consequently, it can be concluded that the remaining 11.5% entered into pathway **II**.

Redoxchemically Induced Reaction. In addition, we also quantified the cross-linking route initiated by **NO+**. In this case, only reaction pathway **II** is addressed. Relative to the calibration system 33% persistent doping charges were deduced, Figure 1a (open black squares). Consequently, 67% of the initial **HMX** radical cations entered reaction pathway **II**.

Figure 1b summarizes the results. It is an important finding that all experiments led to a linear relationship between the mobile charge-carrier density and the amount of initial initiator with a slope of unity. Thus, a constant fraction of the initiator (varies for the different experiments) is transformed to (photochemical initiation) or remains as (redoxchemical initiation) mobile charges that can be detected by the OFET.

3.2. Physical Aspects. The most important result of the previous section is, that cross-linking using a **PAG** or **NO+** leads

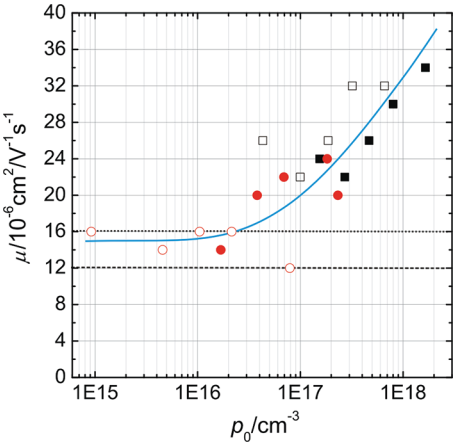

Figure 2. Charge-carrier mobilities of **HMX** (open symbols) and **HM** (closed symbols) as a function of the detected charge-carrier density for different **NO+** (squares) and **PAG** (circles) content, respectively. The blue line is to guide the eye. The dotted line represents the mobility of undoped **HM** and the dashed the mobility of undoped **HMX**.

to significant doping of the semiconductor. Moreover, the formed polymer-network as well as the recombination and decomposition products might also affect the film morphology. Both aspects crucially influence the charge transport and consequently the device performance. The two key parameters characterizing the charge transport are the charge-carrier mobility μ and the permanent charge-carrier density p_0. These parameters were already obtained from the FET experiments and are now examined in detail.

Charge-Carrier Mobility. Figure 2 shows the measured hole mobilities as a function of the charge-carrier density p_0. At low charge-carrier densities the mobility corresponds to the mobility of the undoped hole conductor ($\mu \approx 1.5 \times 10^{-5}$ cm^2 V^{-1} s^{-1}). For p_0 exceeding 3×10^{16} cm^{-3} the mobility increases and reaches $\mu \approx 3.2 \times 10^{-5}$ cm^2 V^{-1} s^{-1} for $p_0 \approx 1 \times 10^{18}$ cm^{-3} ($\triangleq$ 20 wt % doping). This increase by a factor of ca. 2 widely agrees with a study of Maennig et al., who investigated the field-effect mobility of a molecular doped semiconductor.[13] They attributed the increasing mobility with higher doping levels to filling of trap sites.

dx.doi.org/10.1021/cm202327c |*Chem. Mater.* 2011, 23, 5001–5005

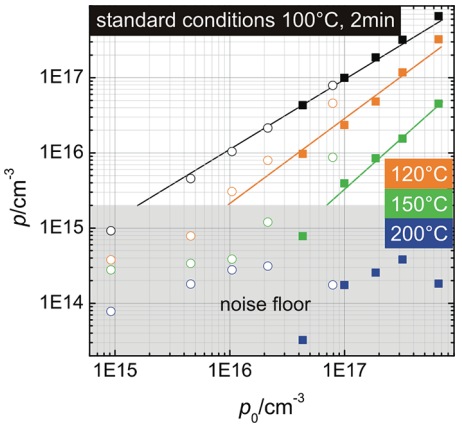

Figure 3. Charge-carrier density of stepwise annealed **HMX** films added with redox-salt (filled squares) **PAG** (open circles), respectively, as a function of the initial charge-carrier density. The films were prepared as described in the Experimental Section (standard conditions) and then heated to 120 °C, 150 °C, and 200 °C for 2 min each. The gray shaded area indicates the resolution limit of the current detection from the transistor characteristics.

Comparing the mobilities of **HM** and **HMX** films added with **PAG** or **NO+** at approximately equivalent doping levels and moderate initiator content we observe no significant difference. This indicates that both **PAG** decomposition product and phenyl adduct do not notably affect the charge transport of the semiconductor for commonly used amounts of **PAG**. Further, we emphasize that in cross-linked **HMX** films the decomposition product of the **PAG** can be washed out by solvent rinsing. However, we also detected no alteration of the mobility as well as the charge-carrier density in such films.

Considering the mobilities of cross-linked and noncross-linked films at equivalent doping levels also yields similar values. Thus, the formation of a cross-linked network does not affect the charge transport. This is expected since **HMX** is an amorphous, highly disordered semiconductor, which should be inherently less sensitive to morphology changes. Further, in particular the long alkoxy side chains should ensure sufficient flexibility of the semiconductor backbone within the rigid polymer network.

Charge-Carrier Density. The charge-carrier density detected by OFET measurements indicates the amount of mobile charge-carriers effectively contributing to the charge transport. Since charge trapping has to be taken into account as well, particularly in disordered systems,[14] doping does not necessarily implicate a quantitative generation of mobile charge-carriers. For quantification, we considered the reference system, i.e., noncross-linkable **HM** doped with **NO+**. The charge-carrier density is given in Figure 1a. With an assumed density of $\delta \approx 1.2$ g/cm^3 we estimated a molecule density of $N = 8 \times 10^{20}$ cm^{-3} for **HM**. From the ratio of the detected density of mobile charge-carriers and the density of doped molecules (N times doping level) we derived a mobile fraction of 1%. Accordingly, only every hundredth doping charge effectively contributes to the charge transport. Similar values were already determined for doped polymers and can be ascribed to strong Coulomb interactions between doping site and the corresponding counterion.[15]

Effective Doping Level. Finally, we can state an effective doping level of cross-linked **HMX** films, which is principally induced by the **PAG**. We know from the reaction pattern that **PAG** stoichiometrically induces 2.5% persistent doping charge. Taking the fraction of effective mobile doping charge into account, i.e. 1%, this leads to an effective doping level of 2.5×10^{-4}. Accordingly, a typical amount of 0.5 wt % **PAG** used for cross-linking[16] would induce 1.7×10^{-6} mobile charge-carriers.

Controlled Dedoping. It has been reported that postbake treatments of cross-linked films lead to dedoping and fluorescence recovery.[17] It is assumed that annealing triggers thermally activated reactions of persistent radical cations, which attack unreacted oxetane units. This leads to a charge transfer to immobile charged sites, such as stable tertiary oxonium ions of ring-opened oxetanes. Figure 3 shows the charge-carrier densities detected by OFET of **HMX** films added with **PAG** or **NO+**, respectively, as a function of the initial charge-carrier density for different annealing temperatures. The charge-carrier density decreases by several orders of magnitude, while the impact is stronger at higher annealing temperatures. Moreover, it is shown, that annealing at 200 °C induces typical charge-carrier densities, which are in the range of undoped samples. This applies to all samples independently of their initial doping level. Furthermore, we emphasize, that increasing the annealing time beyond the standard time used here (10 min) showed no relevant change in the final charge-carrier density. In summary, the dedoping reactions are clearly thermally activated. This is plausible since with higher annealing temperatures the diffusional mobility of reactive moieties is significantly enhanced.

4. CONCLUSION

In conclusion, we report a systematic study of the cross-linking mechanism of oxetane-functionalized semiconductors using a conventional **PAG** and **NO+**, respectively, as initiating species. Persistent doping charge, which is generated during the initiation process, represents an important dead-end, which was detected in OFET devices. Additionally, using a combinatorial experiment all relevant pathways could be quantified. By using **PAG** as initiator the proton formation represents the preferred initiation pathway; simultaneously **PAG** stoichiometrically induces 2.5% persistent doping charge.

The OFET measurements also provided detailed information about the charge transport in doped cross-linked films. The charge-carrier mobility increased with the doping level up to a factor of 2 but showed no significant sensitivity to byproduct or network formation. Further, it turned out that only a fraction of 1% of generated doping charge is effectively mobile. Finally, it was demonstrated that postannealing steps of cross-linked films lead to controlled dedoping.

■ ASSOCIATED CONTENT

Supporting Information. Scheme for CROP (S1), spectra (S2), experimental details (S3), and additional mechanistic studies (S4, S5, and S6). This material is available free of charge via the Internet at http://pubs.acs.org.

■ AUTHOR INFORMATION

Corresponding Author
*E-mail: klaus.meerholz@uni-koeln.de.

■ ACKNOWLEDGMENT

We thank Dr. D. C. Müller (Merck KGaA) for fruitful discussions and the German Federal Ministry of Science and

Education (BMBF) for financial support within the projects HOBBIT and NAPOLI.

REFERENCES

(1) Xiao, L.; Chen, Z.; Qu, B.; Luo, J.; Kong, S.; Gong, Q.; Kido, J. *Adv. Mater.* **2011**, *23*, 926.
(2) Zuniga, C. A.; Barlow, S.; Marder, S. R. *Chem. Mater.* **2011**, *23*, 658.
(3) Huang, F.; Wu, H.; Cao, Y. *Chem. Soc. Rev.* **2010**, *39*, 2500.
(4) Gong, X.; Wang, S.; Moses, D.; Heeger, A. J. *Adv. Mater.* **2005**, *17*, 2053.
(5) Meerholz, K. *Nature* **2005**, *437*, 327.
(6) Zhong, C.; Duan, C.; Huang, F.; Wu, H.; Cao, Y. *Chem. Mater.* **2011**, *23*, 326.
(7) Huang, F.; Cheng, Y.-J.; Zhang, Y.; Liu, M. S.; Jen, A. K.-J. *J. Mater. Chem.* **2008**, *18*, 4495.
(8) Crivello, J. V.; Lam, J. H. W. *Macromolecules* **1977**, *10*, 1307.
(9) Zacharias, P.; Gather, M. C.; Rojahn, M.; Nuyken, O.; Meerholz, K. *Angew. Chem.* **2007**, *46*, 4388.
(10) Devoe, R. J.; Sahyun, M. R. V.; Schmidt, E.; Serpone, N.; Sharma, D. K. *Can. J. Chem.* **1988**, *66*, 319.
(11) Crivello, J. V. *J. Polym. Sci. Part A* **1999**, *37*, 42.
(12) Dektar, J. L.; Hacker, N. P. *J. Org. Chem.* **1990**, *55*, 639.
(13) Pfeiffer, M.; Nollau, A.; Zhou, X.; Leo, K.; Simon, P. *Phys. Rev. B* **2001**, *64*, 195208.
(14) Bässler, H. *Phy. Stat. Sol.* **1993**, *175*, 15.
(15) Zhang, Y.; Blom, P. W. M. *Adv. Funct. Mater.* **2009**, *19*, 1901.
(16) Yang, X.; Müller, C. D.; Neher, D.; Meerholz, K. *Adv. Mater.* **2006**, *18*, 948.
(17) Müller, C. D.; Falcou, A.; Reckefuss, N.; Rojahn, M.; Wiederhirn, V.; Rudati, P.; Frohne, H.; Nuyken, O.; Becker, H.; Meerholz, K. *Nature* **2003**, *421*, 829.